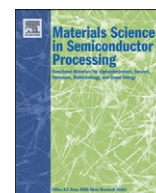


Contents lists available at [SciVerse ScienceDirect](http://SciVerse.Sciencedirect.com)

Materials Science in Semiconductor Processing

journal homepage: www.elsevier.com/locate/mssp

Strain analysis of the GaN epitaxial layers grown on nitridated Si(111) substrate by metal organic chemical vapor deposition

Mustafa K. Ozturk^{a,*}, Engin Arslan^b, İlknur Kars^a, Suleyman Ozcelik^a, Ekmel Ozbay^b^a Department of Physics, Faculty of Science, Gazi University, Teknikokullar, 06500 Ankara, Turkey^b Nanotechnology Research Center-NANOTAM, Department of Physics, Department of Electrical and Electronics Engineering, Bilkent University, 06800 Ankara, Turkey

ARTICLE INFO

Available online 20 July 2012

Keywords:

GaN
AlN layer
MOCVD
Silicon substrates
Strain
Nitridation

ABSTRACT

The strain analysis of GaN film on nitridated Si(111) substrate with different growth times between 0 and 660 s via metal organic chemical vapor deposition (MOCVD) was conducted based on the precise measurement of the lattice parameters by using high-resolution X-ray diffraction (HR-XRD). The nitridation time (NT) was changed at a fixed growth condition. The a- and c-lattice parameters were measured, followed by the in-plane and out-of-plane strains. Then, the biaxial and hydrostatic components were extracted from the total strain values obtained, and were then discussed in the present study as functions of the NT. The biaxial strain and stress are also strongly affected by the non-uniformity of the SiN_x buffer layer thickness.

Published by Elsevier Ltd.

1. Introduction

GaN and its alloys have attracted much attention for optoelectronic device applications because they are very promising materials for a number of devices for optoelectronics and high power–high frequency applications [1–3]. Because of the limited availability of inexpensive homoepitaxial substrates, the GaN films are usually grown heteroepitaxially on sapphire (α -Al₂O₃), SiC, and Si substrates. However, it is difficult to grow high-quality GaN on sapphire, SiC, and Si substrates due to a large lattice mismatch and a thermal expansion coefficient incompatibility and results in a high level of in-plane stress and defects (dislocations, stacking faults, twins, grain boundaries, micropipes, point defects) generation in the GaN epitaxial layer [4–8]. Because of its low cost, large diameter wafer availability with high quality and good thermal and electrical conductivities, Si is regarded as a relatively promising substrate for GaN epitaxy among

these materials. However, the large lattice mismatch and the difference in thermal expansion coefficients between GaN layers and Si substrate lead to the formation of cracks when the thickness of the grown layer exceeds a critical value [5,7,9–11]. The high quality GaN epilayers cannot be grown on these substrates directly. Therefore, several strain compensating layer structures have been offered as buffer layer schemes, such as step-graded AlGaN, AlN, and AlN/GaN or AlGaN/GaN based superlattices and thin silicon nitride (SiN_x) interlayers in order to overcome the problems. The strain compensating buffer layer parameters, such as compound, thickness, and growth temperature, need to be optimized [5,7,9–12]. Wu-Yih Uen et al. [13] investigated the effect of in situ substrate nitridation on the GaN crystalline quality and the nitridation process performed at 750, 950, and 1120 °C, respectively. They demonstrated that the nitridation temperature greatly influences the surface morphology and PL spectra of GaN grown atop the SiN_x buffer layer. Huang et al. [14] reported the growth of a single crystalline GaN films on Si(111) and silicon nitride buffer by hot wall chemical vapor deposition. In their PL measurements, they observe that the insertion of the Si₃N₄ layer removed

* Corresponding author. Tel.: +90 312 2901019; fax: +90 312 2901015.
E-mail address: engina@bilkent.edu.tr (M.K. Ozturk).

the yellow luminescence (YL) peak. And they concluded that the silicon nitride layer not only improved the GaN crystal quality as a growth buffer layer, but also effectively prevented the oxygen and silicon diffusion from the substrate to the epilayer and eliminated YL in GaN epilayers. Wu et al. [15] used the double-buffer structure of AlN/Si₃N₄ in the GaN growth on Si(111) substrate by molecular beam epitaxy (MBE), where single-crystalline Si₃N₄(001) was obtained by introducing the active nitrogen plasma to the Si(111) surface. They demonstrated that an ultra thin (~1.5 nm) Si₃N₄(001) interlayer is very effective in blocking Si/Al inter diffusion during the growth of III-nitrides on Si(111). Hageman et al. [16] showed that the insertion of an SiN_x intermediate layer on a 1 μm GaN layer significantly improves the optical and structural properties of the GaN layer. In our published study, we investigated NT effects on the electrical, optical, and structural properties of GaN epitaxial layers grown on Si(111) substrate [8]. We showed that the SiN_x layer (obtained with in-situ nitridation) affects the surface roughness, dislocation density, and photoluminescence (PL) characteristics of the GaN epitaxial layer [8].

A series of studies were reported on the residual strains and stresses investigations in the GaN epilayer by high-resolution X-ray diffraction measurements [17,19–23]. It was reported that a biaxial strain and a hydrostatic strain could coexist in the GaN epilayer [17,18]. A hydrostatic strain is induced by the presence of point defects, which can be compressive or expansive depending on their size and the biaxial strain by the growth on lattice mismatched substrates with different thermal expansion coefficients [17–23]. The incorporation of doping impurities has two distinct effects on the lattice parameters [24]. The first effect is purely a size effect, which is related to the difference in the atomic radius between the impurity and the host atom that it replaces. The second effect is an electronic effect that is related to deformation potentials [24–26]. The stress in the GaN thin film in GaN/substrate structures, for the given thicknesses of substrate and main epilayer, can be manipulated by the parameters: buffer layer thickness; the buffer layer growth temperature; the compound parameter x of the Ga_{1-x}N_x buffer layer; and the doping level [21–23]. Recently, Cho et al. [21] calculated the strain of a GaN epilayer that was grown on a c-plane sapphire substrate with a different growth time and varying with growth temperature [22]. Harutyunyan et al. [23] published a study describing the high-resolution X-ray diffraction strain-stress analysis of Ga_{1-x}N_x/sapphire heterostructures grown by molecular beam epitaxy (MBE) depending on the relative content of N in the Ga_{1-x}N_x buffer layer with the given thickness and growth conditions.

To our knowledge, there is no strain-stress analysis study on the GaN epilayers grown on nitridated Si(111) substrate by MOCVD. In the present paper, we carried out the strain-stress analysis of GaN/AlN/SiN_x/Si(111) structures depending on the NT length (changes SiN_x buffer thickness) by using High Resolution X-ray Diffraction (HR-XRD). The SiN_x layer was attained easily by a nitridation process in the metal organic chemical vapor deposition (MOCVD) reactor and the nitridation being

performed at different NTs between 0 and 660 s. The c- and a-lattice parameters were measured using HR-XRD, and calculated out-of-plane and in-plane strains. Finally, we obtained the levels of biaxial and hydrostatic components of strain in the GaN epilayer growth on Si(111) substrate.

2. Experimental procedure

GaN epitaxial layers on Si(111) substrate were grown in a low-pressure MOCVD reactor (Aixtron 200/4 HT-S). The reactant source materials for Ga, Al, and N were trimethylgallium (TMGa), trimethylaluminum (TMAI), and NH₃, respectively. The H₂ was used as a carrier gas during AlN and GaN growth. Before loading, the Si substrates were sequentially degreased by H₂SO₄:H₂O₂:H₂O (2:1:1) solutions for 1 min, and etched while in a 2% HF solution for 1 min, rinsed in de-ionized water, and dried with a nitrogen gun. At the beginning of the growth of AlN, the substrate was baked in an H₂ ambient at 1100 °C for 10 min to remove the native oxide. To grow a SiN_x interlayer on an Si(111) substrate surface, following thermal etching, the substrate was nitridated by exposing it to a NH₃ flow of 0.900 slm at 1020 °C. Nitridation was performed at five different times. The NTs were: 0 (without nitridation), 10, 60, 120, 420, and 660 s for samples A, B, C, D, E, and F, respectively. After nitridation, we grew an approximately 150 nm high-temperature (1100 °C) AlN (HT-AlN) buffer layer for all of the samples. In all of the samples, the 250 nm GaN layers were grown at 1050 °C. For sample A, in order to prevent the growth of an amorphous SiN_x interlayer, the technique of the Al pre-covering process of Si substrate was applied before the growth of the AlN buffer [11].

The X-ray measurements were carried out on a Bruker D8-Discover high-resolution diffractometer by using CuKα1 (1.540 Å) radiation, a prodded mirror, and a 4-bounce Ge(220) symmetric monochromator. As regards the Si calibration sample, its best resolution was 16 arc-sec. The double-axis CuKα1 ω–2θ X-ray diffraction spectra were recorded from GaN films for the precise measurement of the a- and c-lattice parameters. We selected two scans from the in and out-planes for exhibiting the quality of the wurtzite hexagonal structure.

3. Analysis of experimental data

The crystallographic structure of GaN belongs to the P6₃mc space group in the hexagonal structure. GaN films in this structure that was grown on c-axis orientated silicon substrate are deformed along the parallel and perpendicular axes with a columnar structure. In this case, the GaN layer introduces a strain that can lead to the cracking of the material, which hardly allows for plastic deformation [27]. The reason for this is the thermal, biaxial strain that was introduced by the different thermal expansion coefficients of the substrate. In general, a GaN layer with a wurtzite structure displays anisotropic behavior, possessing two independent Poisson's ratios. However, the GaN layer displays in-plane quasicubic (isotropic) elastic behavior with respect to

hydrostatic pressure, which comes from the point defects. Its in-plane deformation state can be described by one strain component [18,19,22,23]. Therefore, out-of-plane, ε_c , and in-plane, ε_a , strain components of the GaN layer can be expressed as,

$$\begin{aligned}\varepsilon_c &= \frac{c_r}{c_0} - 1 \\ \varepsilon_a &= \frac{a_r}{a_0} - 1\end{aligned}\quad (1)$$

where c_r and a_r are strained lattice parameters, and c_0 and a_0 are unstrained lattice parameters [17,22,23]. The real value, c_r , of the c -lattice parameter and its experimental values, $\{c_l\}$, are connected with Equation given below,

$$c_l = -\frac{Dc_r \cos^2 \theta_l}{r \sin \theta_l} + c_r \quad (2)$$

c_l value can be calculated from the peak position (hkl) reflection. r (~ 415 mm) is the distance specimen detector, D ($\sim 0.15^\circ$) is the possible displacement of the specimen with respect to the goniometer axis in the equatorial plane and the lattice parameter c_r is determined from the plots $\{\theta_l, c_l\}$ ($l=2, 4, 6$) [23,29].

The c_l -lattice parameter of GaN film was calculated by using the ω - 2θ -scans of the (000 l) reflections for $l=2, 4, 6$.

$$c_l = \frac{l\lambda}{2\sin\theta_l} \quad (3)$$

where, θ_l is the peak position of the GaN (000 l) reflection, and λ is the wavelength of the $CuK_{\alpha 1}$ reflection. Harutyunyan et al. [23] used the c_l -lattice parameters in order to obtain an ideal lattice parameter c_r , determining a-lattice parameter with their averaging values. Then, the out of plane strain component, ε_c , is determined from Eq. 1 for the average value \bar{c}_r and the unstrained lattice parameter $c_0=0.51855$ nm measured for powder GaN [28]. The calculated values of the parameters, c_r , \bar{c}_r are shown in Table 1.

The a-lattice parameter of the GaN film for the diffraction peaks of the asymmetrical reflections (hkl) is given by

Table 1

The values c_r (measured for a certain azimuthal position of the sample) and \bar{c}_r of GaN epilayer in GaN/AlN/SiN_x/Si(111) structures as a function of NT.

Nitridation Time (s)	Diffraction peak position, θ_l^a			Measured c-lattice parameter order of the reflection, c^a (nm)	
	$l=2$	$l=4$	$l=6$	c_r	\bar{c}_r
0	17.239	36.459	63.096	0.51867	0.51867
10	17.413	36.621	63.265	0.51608	0.51608
60	17.281	36.484	63.134	0.51810	0.51810
120	17.278	36.478	63.108	0.51820	0.51820
420	17.378	36.135	63.292	0.51837	0.51837
660	17.402	36.592	63.219	0.51637	0.51637

^a The error interval for the peak positions (θ_l) is ± 0.002 and the error value of the c -lattice parameter is ± 0.00001 .

the below Equation;

$$a^{(hkl)} = cd_{hkl} \sqrt{\frac{(4/3)(h^2 + k^2 + hk)}{c^2 - l^2 d_{hkl}^2}} \quad (4)$$

where $c \equiv \bar{c}_r$ over the four different azimuthal positions and d_{hkl} is the distance of the interplanes of (hkl) reflecting atomic planes as determined from the θ_l angular position of the diffraction peak and $c \equiv c_r$. The calculated a-lattice parameter values are given in Table 2. In an analogous way, the in-plane strain is obtained from Eq. 1 by using $a_0=0.31878$ nm for the unstrained a-lattice parameter [23,29].

4. Results and discussion

Fig. 1 plots a ω - 2θ profile of the GaN layer grown on an AlN buffer layer deposited on nitridated Si (111) substrate for sample F. As shown in Fig. 1, beside the Si (111) and AlN (0002) reflections, an intense GaN (0002) reflection was observed only at $\theta = 17.3^\circ$, indicating that the GaN has a single phase of wurtzite structure.

In Fig. 2, the azimuths of the GaN (12 $\bar{3}$ 1) plane recorded for sample F is shown, since these results are representative. Azimuths repeat every 60° between -90 and $+90$ with varying intensity values showing an inclination of azimuth planes perpendicular to the (12 $\bar{3}$ 1) plane. For the strain analysis, we used the (0002), (0004), (0006), (10 $\bar{1}$ 5), (20 $\bar{2}$ 2), (12 $\bar{3}$ 1), 10 $\bar{1}$ 1, (10 $\bar{1}$ 3), and (11 $\bar{2}$ 4) reflections.

The external biaxial strain originates from the lattice-mismatched substrates and from the post-growth cooling [18,19]. The effective a-lattice parameter of GaN is larger than that of silicon substrate. Therefore, compressive stress can be induced in the GaN epilayer. In the GaN epilayer, the measured total strains in the a and c-directions change as both tensile (positive strain) and compressive (negative strain) type, and strongly exhibits an NT dependent behavior as shown in Fig. 3. However, the strain in the c-direction develops in the compressive region. They increase or decrease firstly with the NT, and then decrease or increase, respectively. From this point, one can see a monotonic increase or decrease, respectively, for every two strains in the GaN epilayer upon increasing the NT. As shown in Fig. 3, the deformation state of a GaN epilayer essentially depends on the NT. This case may happen because the nonuniform SiN_x buffer layer thickness could prevent dislocation motion parallel to the (0001) lattice planes [30]. In addition, the deformation states in the GaN epilayer appeared with point defects that originated from the large difference in the covalent radii of the Ga and the N atoms ($r_{Ga}=0.126$ nm, $r_N=0.07$ nm). Furthermore, it can be affected by common impurities or doping materials (oxygen, elements to induce n or p -type carriers) if they are used in the growth of films.

The GaN layer of the GaN/Si structures grown by the MOCVD and MBE contains a high concentration of point defects which cause a considerable contraction or expansion of the crystal lattice in this layer [18,19,21,23]. Because of this reason, out-of-plane and in-plane strain

Table 2The value of the a-lattice parameter of the GaN epilayer in GaN/AlN/SiN_x/Si(111) structures as a function of NT.

Diffraction peak position θ_{hkl}^a for reflection (hk(-h-k)l)										a ^a -lattice parameter
Nitridation Time (s)	(10.1)	(10.2)	(10.5)	(11.2)	(11.4)	(12.1)	(20.1)	(20.2)	(20.3)	(nm)
0	18.498	24.080	52.589	34.813	49.868	48.581	35.152	39.084	45.476	0.31819
10	18.359	23.988	52.535	34.552	48.722	48.693	35.554	39.343	45.771	0.32208
60	18.705	24.047	52.669	34.440	49.967	49.193	35.669	39.609	45.828	0.31660
120	18.665	24.286	52.661	34.806	50.128	49.059	35.520	39.388	45.710	0.31584
420	18.364	24.030	52.626	34.507	49.997	48.791	35.310	39.055	45.494	0.31870
660	18.343	24.063	52.504	34.553	49.952	48.863	35.240	39.203	45.590	0.32051

^a The error interval for the peak positions (θ_{hkl}) is ± 0.002 and the error value of the a-lattice parameter is ± 0.00001 .

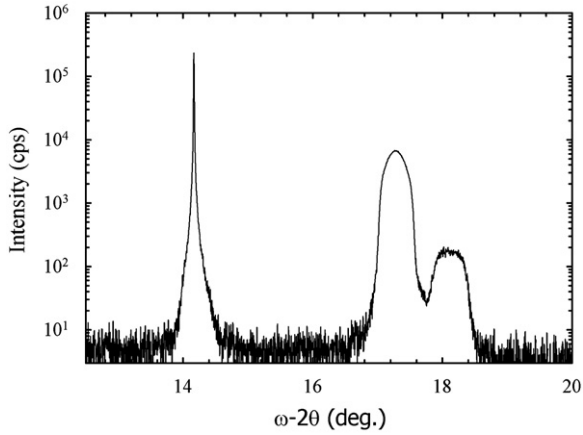


Fig. 1. The ω - 2θ -scans pattern of the sample F (GaN epilayer grown on an Si (111) substrate with a 660 s NT) obtained by using a four-Ge(022) crystal monochromator.

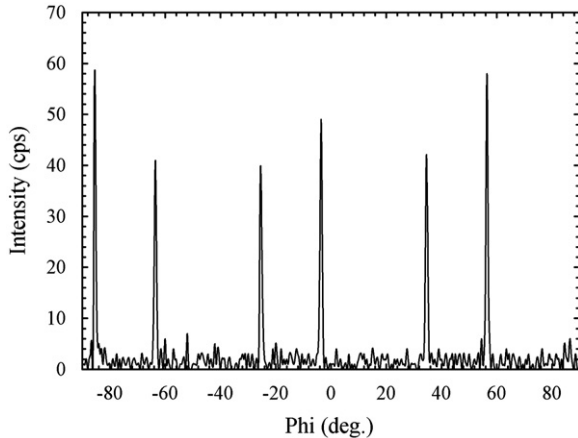


Fig. 2. Phi scan curve of asymmetric GaN ($12\bar{3}1$) and AlN ($12\bar{3}1$) reflection planes for sample F. Every peak shows the azimuths of the ($12\bar{3}1$) planes. The diffractive peaks for the AlN and GaN repeat every 60° .

components in the GaN layer are the superposition of biaxial and hydrostatic strains [18,19,21,23],

$$\varepsilon_c = \varepsilon_c^b + \varepsilon_h$$

$$\varepsilon_a = \varepsilon_a^b + \varepsilon_h \quad (5)$$

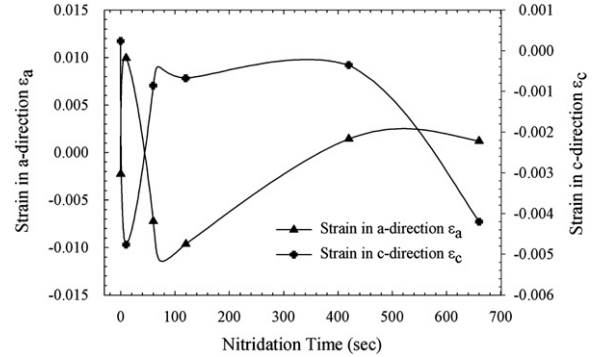


Fig. 3. The measured strain in the a- and c-directions of the GaN epilayer in GaN/AlN/SiN_x/Si(111) structures as a functions of the NT.

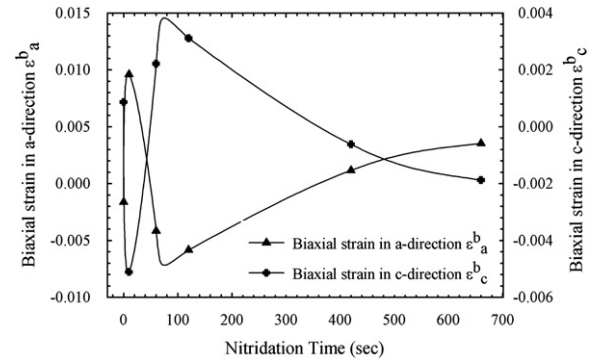


Fig. 4. The measured biaxial strain in the a- and c-directions of the GaN epilayer in GaN/AlN/SiN_x/Si(111) structures structure as a function of NT.

In these Equations, the ε_c^b and ε_a^b are the biaxial strains in the c- and a-direction, respectively. The hydrostatic strain component ε_h is given by

$$\varepsilon_h = \frac{1-\nu}{1+\nu} \left(\varepsilon_c + \frac{2\nu}{1-\nu} \varepsilon_a \right) \quad (6)$$

where, ν is the Poisson ratio, which is determined from the elastic constants of the GaN layer, c_{13} and c_{33} with the Equation $\nu = c_{13}/(c_{13} + c_{33})$. Their values for GaN layer, $c_{13} = 106$ GPa and $c_{33} = 398$ GPa, were taken from what was cited in the previous report [23,31,32]. Figs. 4 and 5 show the out-of-plane (in the c-direction) and in-plane

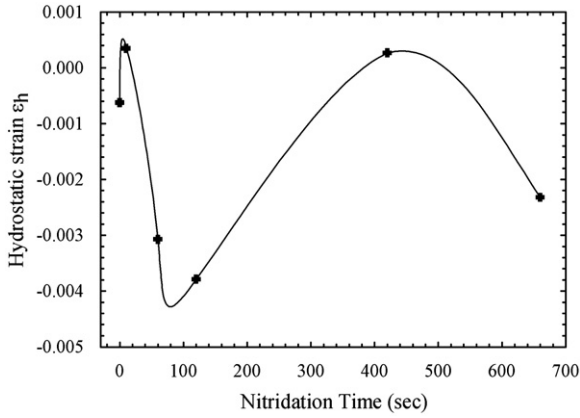


Fig. 5. Behavior of the measured hydrostatic strain, ε_h , of the GaN epilayer in GaN/AlN/SiN_x/Si(111) structures as a function of NT.

(in the a-direction) biaxial strain components ε_c^b and ε_a^b , as well as the hydrostatic strain ε_h .

Biaxial strains ε_a^b , ε_c^b in the a- and c-directions, respectively, come from the growth on the lattice-mismatched silicon substrate and post growth cooling, depending on the NT. The measured biaxial strains of the GaN layers are shown in Fig. 4 as a function of the NT. A strong NT-dependent trend is observed in every two directions. We obtained compressive a- and tensile c-biaxial strain values -1.62×10^{-3} and 8.62×10^{-4} for sample A (without nitridation). The a-biaxial strain increases with the NT and comes to a minimum value of 9.60×10^{-3} and then decreases to -5.83×10^{-3} . From this point, one can see a monotonic increase of the a-biaxial strain in GaN upon increasing NT. The c-biaxial strain shows inverse behavior due to the a-biaxial strain. It comes to a minimum -5.11×10^{-3} and then increases to 3.11×10^{-3} . The lattice mismatch between Si and GaN is nearly 16%, which causes a high dislocation density in the GaN layers, but the major problem is the thermal mismatch, which is 54% [30]. Therefore, thick epilayers of the GaN for device fabrication are not achievable without cracks. Even if Mismatch, with an AlN sublayer, is also reduced to 2.4% [30] and the thickness of GaN is fixed to 250 nm, the cracks of GaN are not prevented. The biaxial strain in the a-direction in Fig. 4 does not agree with the -0.002 value of the calculated thermal strain, except for sample A. However, the value of sample A is close to the thermal strain. For other samples, these results are also expected because stress and strain are affected strongly by nitridation.

It is commonly known that hydrostatic strain comes from N_{Ga} and Ga_N substitutional type point defects, N_i and Ga_i interstitial point defects, and V_N and V_{Ga} vacancies if the covalent radius of the Ga atom is considerably larger than the covalent radius of the N atom. Therefore, the Ga_N , Ga_i and N_i type defects cause a crystal lattice expansion, whereas N_{Ga} , V_{Ga} and V_N type point defects lead to crystal lattice compression [23]. Here, the general behavior that is similar to that of the measured strains is also observed for the hydrostatic strain. As can be seen in Fig. 5, the

hydrostatic strain exhibits oscillation with large amplitude and has a compressive character for other samples except for samples B and E in the compressive type. There is no systematic dependence on the NT. The compressive hydrostatic strains for samples A, C, D, and F suggest that the relative concentration of the Ga_N , Ga_i and N_i type defects are more dominant. On the other hand, the Ga_N , Ga_i , N_i , O_i and C_i type defects, for samples B and E can be thought to have caused a crystal expansion [22,23].

In the GaN/Si(111) structures, the character of the stress is really biaxial and caused by the mismatch between the epilayer and the substrate lattice parameters [17,20,22,23,30]. The in-plane biaxial stress in the GaN epilayer σ_f can be calculated by the relationship [20,22,23].

$$\sigma_f = M_f \varepsilon_a^b \quad (7)$$

Where M_f is the biaxial elastic modulus, which is determined by [20,22,23].

$$M_f = c_{11} + c_{12} - 2 \frac{c_{13}^2}{c_{33}} \quad (8)$$

The elastic constants of wurtzite GaN, c_{ij} , from the Brillouin scattering measurement, were used as $c_{11} = 390$ GPa, $c_{12} = 145$ GPa, $c_{13} = 106$ GPa and $c_{33} = 398$ GPa, respectively. Using these data for c_{ij} , the value $M_f = 478.5$ GPa is obtained for the biaxial elastic modulus [23,31]. The biaxial stress component in the c-direction equals zero [22,23,32]. The data for σ_f as a function of NTs are given in Fig. 6. As can be seen in Fig. 6, the biaxial stress, σ_f , increases with the NT and arrives at a minimum value of 4.59 Gpa and then decreases to -2.79 Gpa. After this point, a monotonic increase of biaxial stress in the GaN layer upon an increasing NT is observed. The tensile biaxial stress is affected by the thermal expansion coefficient of SiN_x.

The thermal expansion coefficient for the silicon substrate is $\alpha_{Si} = 2.6 \times 10^{-6} \text{ K}^{-1}$, which is smaller than those ($\alpha_{GaN} = 5.6 \times 10^{-6} \text{ K}^{-1}$) of GaN and ($\alpha_{AlN} = 4.6 \times 10^{-6}$) of AlN at room temperature as well as at the growth temperature ($\alpha_{GaN} = 5.4 \times 10^{-6} \text{ K}^{-1}$, $\alpha_{AlN} = 6.9 \times 10^{-6} \text{ K}^{-1}$, $\alpha_{Si} = 4.4 \times 10^{-6} \text{ K}^{-1}$) [30,33–35]. These large thermal differences induce

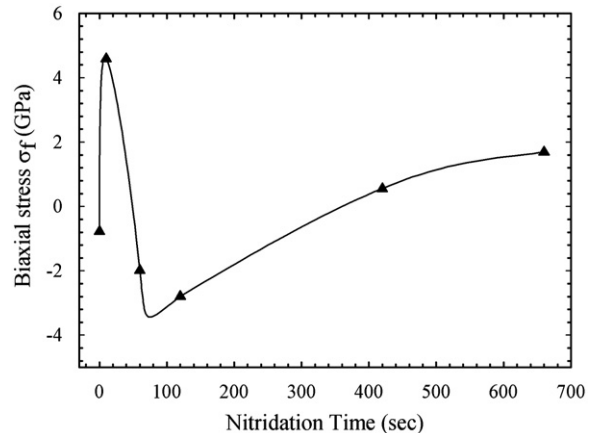


Fig. 6. The measured biaxial stress, σ_f , in GaN epilayer in GaN/AlN/SiN_x/Si(111) structures as a function of NT.

compressive stress in the GaN layer [22,23]. The thermal strain was calculated as $\varepsilon_{thermal} = (\alpha_{Si} - \alpha_{GaN})\Delta T$ and the value is the -0.002 , where α_{Si} and α_{GaN} are the thermal expansion coefficients of Si and GaN, respectively, in which ΔT is the difference between the growth temperature and room temperature. This value is a little larger than what is typical for the samples grown on an Al_2O_3 substrate [36]. The origination of thermal strain is the post growth cooling from the growth temperature $1050^\circ C$ to room temperature.

5. Conclusion

All of the samples with different NTs showed a general behavior for the calculated strains and stress. This behavior strongly originated from varying the NTs. The mean lattice parameters in the a- and c-directions were obtained from the peak positions of symmetric and asymmetric reflection planes. From these lattice parameters, the measured strains in the a- and c-directions, biaxial strains, and hydrostatic strain are calculated by using Kisielowski's Equations. The calculations show that the total strain comprises the sum of the biaxial and hydrostatic. The biaxial strain and stress are also strongly affected by the non-uniformity of the SiN_x buffer layer thickness. The calculations of the hydrostatic strain result in the fact that the relative concentration of the GaN , Ga_i and N_i type defects are more dominant.

Acknowledgments

This work is supported by the European Union under the projects EU-METAMORPHOSE, EU-PHOREMOST, EU-PHROME, and EU-ECONAM, and TUBITAK under Project Numbers 105E066, 105A005, 106E198, 106A017, and 107A012. One of the authors (E.O.) also acknowledges partial support from the Turkish Academy of Sciences.

References

- [1] S.N. Mohammad, A. Salvador, H. Morkoç, Proceedings of the IEEE 83 (1996) 1420–1422.
- [2] L. Shen, S. Heikman, B. Moran, R. Coffie, N.Q. Zhang, D. Buttari, I.P. Smorchkova, S. Keller, S.P. DenBaars, U.K. Mishra, IEEE Electron Device Letters 22 (2001) 457–459.
- [3] A. Dadgar, M. Poschenriender, J. Blasing, O. Contreras, F. Bertram, T. Riemann, A. Rieher, M. Kunze, I. Daumiller, A. Krtschil, A. Diez, A. Kaluza, A. Modlich, M. Kamp, J. Christen, F.A. Ponce, E. Kohn, A. Krost, Journal of Crystal Growth 248 (2003) 556–562.
- [4] J. Narayan, P. Pant, A. Chugh, H. Choi, J.C.C. Fan, Journal of Applied Physics 99 (054313) (2006) 1–7.
- [5] E. Arslan, M.K. Ozturk, Ö. Duyugulu, A.A. Kaya, S. Ozcelik, E. Ozbay, Applied Physics A-Materials Science and Processing 94 (2009) 73–82.
- [6] A.M. Roskowsky, E.A. Preble, S. Einfeldt, P.M. Miraglia, J. Schick, R. Grober, R.F. Davis, Opto-Electronics Review 10 (2002) 261–270.
- [7] E. Arslan, M.K. Ozturk, S. Ozcelik, E. Ozbay, Current Applied Physics 9 (2) (2009) 472–477.
- [8] E. Arslan, Ö. Duyugulu, A.A. Kaya, A. Teke, S. Özçelik, E. Ozbay, Superlattices and Microstructures 46 (2009) 846–857.
- [9] A. Krost, A. Dadgar, G. Strassburger, R. Clos, Physica Status Solidi (a) 200 (2003) 26–35.
- [10] J. Blasing, A. Reiher, A. Dadgar, A. Diez, A. Krost, Applied Physics Letters 81 (2722) (2002) 1–3.
- [11] E. Arslan, M.K. Ozturk, A. Teke, S. Ozcelik, E. Ozbay, Journal of Physics D: Applied Physics 41 (155317) (2008) 1–10.
- [12] K. Cheng, M. Leys, S. Degroote, B. Vandaele, S. Boeykens, J. Derluyn, M. Germain, G. Vantendeloo, J. Engelen, G. Borghs, Journal of Electronic Materials 35 (2006) 592–598.
- [13] Zhen-Yu Wu-Yih Uen, Shan-Ming Li, Sen-Mao Lan, Liao, Journal of Crystal Growth 280 (2005) 335–340.
- [14] J. Huang, Z. Ye, L. Wang, J. Yuan, B. Zhao, H. Lu, Solid-State Electronics 46 (2002) 1231–1234.
- [15] C.L. Wu, J.C. Wang, M.H. Chan, T.T. Chen, S. Gwo, Applied Physics Letters 83 (2003) 4530–4532.
- [16] P.R. Hageman, S. Haffouz, V. Kirilyuk, A. Grzegorzczak, P.K. Larsen, Physica Status Solidi (a) 188 (2001) 523–526.
- [17] C. Kisielowski, J. Kruger, S. Ruvimov, T. Suski, J.W. Ager, E. Jones, Z.L. Weber, M. Rubin, E.R. Weber, M.D. Bremser, R.F. Davis, Physical Review B 54 (1996) 17745–17753.
- [18] C. Kisielowski, Semiconductors and Semimetals 57 (1998) 275–317.
- [19] S. Raghavan, J. Acord, J.M. Redwing, Applied Physics Letters 86 (261907) (2005) 1–3.
- [20] S. Raghavan, J. Redwing, Journal of Applied Physics 98 (023515) (2005) 1–8.
- [21] S.I. Cho, K. Chang, M.S. Kwon, Journal of Materials Science 43 (2008) 406–408.
- [22] S.I. Cho, K. Chang, M.S. Kwon, Journal of Materials Science 42 (2007) 3569–3572.
- [23] V.S. Harutyunyan, A.P. Aivazyan, E.R. Weber, Y. Kim, Y. Park, S.G. Subramanya, Journal of Physics D: Applied Physics 34 (2001) A35–A39.
- [24] G. Chris, Walle Van de, Physical Review B 68 (165209) (2003) 1–5.
- [25] J. Neugebauer, Chris G Van de Walle, Physical Review B 50 (1994) 8067–8070.
- [26] M.A. Reshchikov, G.C. Yi, B.W. Wessels, Physical Review B 59 (1999) 13176–13183.
- [27] T. Ive, O. Brandt, K.H. Ploog, Journal of Crystal Growth 278 (2005) 355–360.
- [28] C. Balkas, C. Basceri, R. Davis, Powder Diffraction 10 (1995) 266–268.
- [29] Y.S. Umanskii, Y.A. Skakov, A.N. Ivanov, L.N. Rastorguyev, Crystallography, Rentgenography and Electron Microscopy, Metalurgiya, Moscow, 1982.
- [30] S. Kaiser, M. Jakob, J. Zweck, W. Gebhardt, Journal of Vacuum Science and Technology B 18 (2000) 733–741.
- [31] A. Polian, M. Grimsditch, I.G. Grzegory, Journal of Applied Physics 79 (1996) 3343–3344.
- [32] M.A. Moram, Z.H. Barber, C.J. Humphreys, Journal of Applied Physics 102 (023505) (2007) 1–4.
- [33] S. Pal, C. Jacob, Bulletin of Material Science 27 (2004) 501–504.
- [34] K. Wang, R.R. Keeber, Materials Research Society Symposium Proceedings 482 (1998) 863–868.
- [35] G.A. Slack, S.F. Bartram, Journal of Applied Physics 46 (1975) 89–99.
- [36] D.H. Shin, M.K. Bae, S.N. Yi, J.H. Na, A.M. Gren, R.A. Taylor, Y.J. Cho, H.M. Cho, S.H. Park, Journal of the Korean Physical Society 48 (2006) 1255–1258.